RADIO: Effective and Efficient Anomalous Subgraph Discovery in Financial Networks

Xiaolin Han[1,2], Yikun Zhang[1], Chenhao Ma[3], Lingyun Song[1], and Xuequn Shang[1(✉)]

[1] Northwestern Polytechnical University, Xi'an, China
{xiaolinh,lysong,shang}@nwpu.edu.cn, {yikunzhang}@mail.nwpu.edu.cn
[2] Laboratory for Advanced Computing and Intelligence Engineering
[3] Chinese University of Hong Kong, Shenzhen, China machenhao@cuhk.edu.cn

Abstract. Detecting abnormal subgraphs is crucial for structural-level anomaly detection, offering insights into atypical interactions overlooked by traditional single-node anomaly detection methods, particularly crucial in financial networks for spotting potential money laundering activities. Current challenges arise from the diverse and complex transaction distributions and the vast scale of real-world financial networks. Addressing these, we propose a novel Reinforcement-based Anomalous subgraph DIscOvery algorithm (**RADIO**). RADIO incorporates an innovative subgraph encoder along with a coarse prototype discovery module, enabling efficient and accurate identification of anomalous subgraphs amidst intricate transaction distributions. It further enhances subgraph detection through strategic reward design, directing optimization towards the most significant abnormalities. Our comprehensive evaluation, using four real financial transaction datasets and comparing with twelve existing methods, confirms its exceptional performance. It outperforms the current state-of-the-art approach by an average of 7× in abnormal degrees of detected subgraphs and demonstrates high efficiency in handling networks with millions of nodes.

Keywords: Anomalous subgraph discovery · Reinforcement learning.

1 Introduction

Detecting abnormal subgraphs in financial networks is an important problem [3, 12, 13]. This problem is often used to detect fraud and money laundering behaviors. For example, the banking sector can detect these criminals transferring illegal money to untraceable accounts, thereby preventing financial fraud[12]. Specifically, this paper explores the detection of subgraph patterns that significantly deviate from normal behaviors. Given a graph with node set V, an anomaly is a subgraph with node set $S \subseteq V$ that deviates significantly from normal ones with respect to graph structure and transaction information.

In the existing literature, most anomaly discovery solutions [12, 13] only consider the structural information while ignoring the associated transaction information of money laundering. However, some subgraphs may be normal if their

transactions are legal. For example, the university account distributes scholarships, allowances, etc., to student accounts, and student accounts transfer tuition fees, dormitory fees, etc., to the university account.

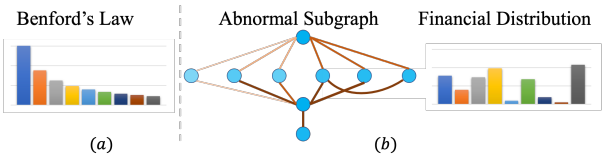

Fig. 1. (a) Benford's law; (b) abnormal subgraph with financial distribution.

To measure transaction irregularities, the state-of-the-art method AntiBenford [3] leverages Benford's law—also known as the Newcomb-Benford law [1, 3]—which states that the fraction of numbers starting with the digit o follows a monotonic decreasing function of o (as illustrated in Figure 1(a)), i.e., $\log_{10}(1+1/o)$, in real-world datasets such as tax records, stock quotations, et al [3]. AntiBenford applies this law to detect abnormalities in transactional data by calculating the first digit distribution, i.e., financial distribution, of the subgraph. Here, the abnormal subgraph (with edge colors representing transaction frequency) shown in Figure 1(b) reveals a dense set of transactions with its financial distribution significantly deviating from Benford's law, signaling potential anomalies.

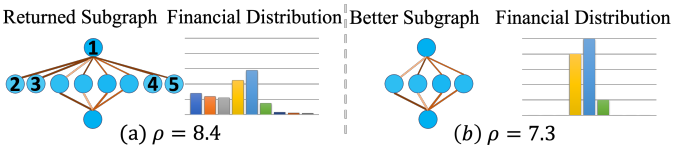

Fig. 2. (a) The returned subgraph with a density of 8.4; (b) the better subgraph with a density of 7.3 but deviates from Benford's law more significantly.

While AntiBenford [3] represents a significant advancement in anomaly discovery by utilizing both structural and transactional information to identify dense subgraphs deviating from Benford's law, it exhibits certain limitations. AntiBenford identifies dense subgraphs that deviate from Benford's law, but some nodes within these dense regions may include legally normal transactions. For example, in Figure 2, node 1 frequently makes payments to nodes {2, 3, 4, 5} (representing daily expenses at restaurants and supermarkets), which are legal transactions. This approach misses more subtly deviant subgraphs. Specifically, in Figure 2(a), AntiBenford identifies the densest subgraph with a density score of 8.4. Yet, its subgraph, shown in Figure 2(b), is a better choice with a

lower density of 7.3 but a higher deviation from Benford's law. This necessitates refining candidate subgraphs by exploring potentially more abnormal subgraphs.

Another limitation arises from the computational demands of calculating Benford deviations across all candidate subgraphs. AntiBenford assesses each candidate sequentially, which becomes a bottleneck as the required number of abnormal subgraphs increases. For instance, identifying 800 abnormal subgraphs in Ethereum's financial network from January 2018 took 32.8 hours—an impractically long processing time for real-time detection needs, such as timely tracking of money laundering. These issues call for a more *effective* and *efficient* solution in discovering abnormal subgraphs.

Our contributions. Our first goal is to develop effective abnormal subgraph discovery methods, which is challenging due to the intricate graph structure and diverse financial distribution in networks. We tackle this challenge by introducing a novel learning-based approach, RADIO. The novelty of our approach lies in its ability to optimize approximations towards more abnormal directions, resulting in superior results compared to traditional algorithms. Moreover, we capture hidden features behind abnormal subgraphs, which is non-trivial. Specifically, we propose a novel subgraph encoder to extract the hidden features from the graph structure. Besides, we propose measuring similarity among financial distributions of subgraphs using KL-divergence. This enables embedding subgraphs with similar graph structures and close financial distributions nearly in the feature space.

Second, we focus on accelerating the abnormal subgraph discovery process, which is a challenging task, particularly in large financial networks where calculating candidate subgraphs for every node results in excessive and unnecessary computations. Hence, we propose a pruning strategy to expedite the process. Specifically, we only retain the top-p dense subgraphs with significant deviations from Benford's law for further refinement. Additionally, we leverage multiprocessors to compute candidate subgraphs in parallel, accelerating the acquisition of coarse prototypes. Moreover, we introduce a reinforcement learning algorithm to refine the subgraphs efficiently, where the learnable parameters can be trained offline. These strategies minimize unnecessary computation for normal subgraphs and facilitate efficient learning-based refinement for all abnormal subgraphs simultaneously, rather than sequentially. Consequently, we can efficiently discover all abnormal subgraphs concurrently. For example, RADIO detected 800 abnormal subgraphs from the large Ethereum network within 2.6 hours during January 2018, which is 12.6 times faster than the SOTA method AntiBenford.

We have performed substantial experiments on four real financial datasets against twelve baselines. Compared with the SOTA, RADIO achieves 7× improvement on average w.r.t. the abnormal degree, and ten times faster in large financial networks where the number of required abnormal subgraphs is large, e.g., over 500. RADIO is also scalable on large financial networks.

2 Related Work

Non-learning-based anomaly detection. Graphs are prevalent in many data mining tasks [6–9, 16, 17, 19, 18, 25, 26]. Eigenspokes [22] proposes to extract surprising patterns for scalable community chipping discovery. Holoscope [13] extracts the contrast patterns between nodes by using topology and spikes in graphs. FlowScope [12] uses multipartite graphs to detect the complete flow of money with a scalable algorithm. The SOTA method AntiBenford [3] first finds the densest subgraphs in the network, then filters out subgraphs that are not statistically significant anomalous. However, these methods suffer from efficiency problems when the number of abnormal subgraphs is large.

Learning-based anomaly detection. Learning-based methods utilize machine learning or deep learning to learn latent features behind subgraphs and use these features to detect communities or anomalies [24]. SEAL [30] proposes generative adversarial networks for community detection by learning heuristics. BigClam [29] is proposed to detect communities by a nonnegative matrix factorization approach. However, it cannot capture diverse edge distribution among nodes. CPM [21] proposes a clique percolation method for community structure discovery. It identifies communities by finding connections between cliques that share nodes. The advanced method CLARE [28] proposes to learn hidden features behind the anomalous communities, and use a reinforcement-learning framework to detect anomalies. AS-GAE [31] proposes to extract the anomalous subgraphs in an unsupervised framework. GCAD [33] regards h-subgraphs that are scarce and different from the majority of h-subgraphs as anomalies. SIGNET [14] proposes to learn the most discriminative motifs of graph samples that can explain the anomaly of graphs.

Densest subgraph discovery. Several methods study undirected densest subgraph discovery: Density-Friendly [4] uses the Frank-Wolfe algorithm, Core-Exact [5] employs clique-based cores. For directed subgraphs, Core-Approx [18] utilizes a core-based approximation algorithm, while KS-Approx [10] offers a max-flow-based solution for at least and at most subgraph problems. However, these methods, designed for general graphs, may not effectively capture the intricate transaction distribution among nodes.

3 Problem Definition

Definition 1 (Financial Network) *A financial network is a graph $G(V, E, w_m)$, where V is the set of nodes, $E = \{(i, j) \in V \times V : i \mapsto j\}$ is the set of edges, and $w_m(u, v)$ denotes the edge weight (i.e., the amount of money that node u sends to v).* □

Definition 2 (Benford's law[1, 3]) *Benford's law is the distribution of the first digit of numbers appearing in a wide variety of numerical data.* □

Problem Definition: Anomalous subgraph discovery problem [3]. Given a financial network $G(V, E, w_m)$, the goal is to identify anomalous subgraphs,

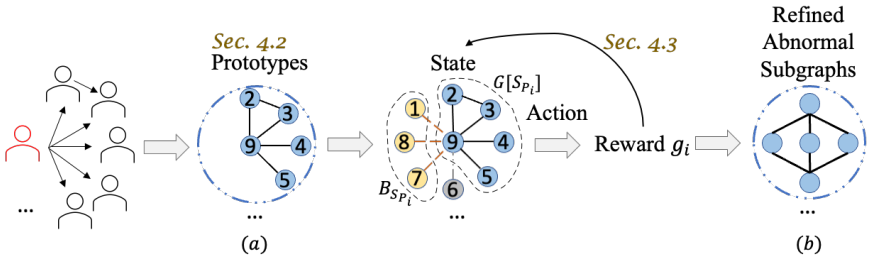

Fig. 3. The overall framework of the RADIO model, where $G[S_{P_i}]$ denotes the prototype obtained by the coarse prototype discovery in Sec. 4.2, and $B_{S_{P_i}}$ denotes the boundary of the subgraph $G[S_{P_i}]$.

each involving a subset of nodes $S \subseteq V$ such that (i) its induced subgraph has a high density, and (ii) whose financial distribution $w(G[S])$ deviates from Benford's law significantly in statistics. The financial distribution $w(G[S])$ is computed by extracting the first digits from the edge weights w_m within the subgraph $G[S]$ and constructing a histogram of their frequencies.

4 The RADIO Model

4.1 Framework

Figure 3 shows the overall framework. Initially, the *coarse prototype discovery* module efficiently identifies rough abnormal prototypes (Figure 3 (a)) in financial networks (Section 4.2). Then, the *anomalous subgraph refinement* refines the abnormal prototypes using a novel reinforcement learning framework (Section 4.3) and obtains the refined abnormal subgraphs (Figure 3 (b)).

4.2 Coarse Prototype Discovery

We propose a top-p coarse prototype discovery approach for fast abnormal candidates detection as follows.

Prototype discovery. Firstly, for each node $v \in V$ in the financial network, we construct its k-ego net. We then apply a fast approximate densest subgraph discovery algorithm [2] on each k-ego net, which operates with linear time complexity. It involves iteratively peeling the k-ego net by removing the node with the smallest degree and recalculating the density $\rho(S) = \frac{|E(S)|}{|S|}$ of the remaining graph until $S = \emptyset$. The subgraph with the highest density $\rho(S)$ observed during this process is identified as the approximate densest subgraph $G[\widehat{S}]$.

Corollary 1. *The subgraph returned by the peeling process has a density of at least* $\frac{1}{2}$ *of the densest subgraph induced by any subset of the node set* V_k *of the* k*-ego net.*

Second, we employ an early pruning strategy to find the top-p abnormal subgraphs from the approximated densest subgraphs if they deviate from Benford's law significantly. To measure the deviation degree from Benford's law, we utilize the $\mathcal{X}^2(\widehat{S})$-statistic, $\widehat{S} \subseteq V$, which calculates the deviation between the actual distribution in the subgraph $G[\widehat{S}]$ and the expected Benford's distribution as:

$$\mathcal{X}^2(\widehat{S}) = \sum_{o=1}^{O} \frac{\left(d_{\widehat{S},o} - \mathbb{E}(d_{\widehat{S},o})\right)^2}{\mathbb{E}(d_{\widehat{S},o})}\ , \tag{1}$$

where $d_{\widehat{S},o}$ denotes the number of edges in the subgraph $G[\widehat{S}]$ whose transaction amount's first digit equals $o \in \{1, \cdots, 9\}$, and $\mathbb{E}(d_{\widehat{S},o})$ represents the expected number of edges whose transaction amount's first digit equals o based on Benford's law.

Theorem 1. *An anomalous subgraph is a subset of nodes $\widehat{S} \subseteq V_k$ such that $\mathcal{X}^2(\widehat{S}) \gg 2\rho(\widehat{S})|\widehat{S}|$.*

According to Theorem 1, anomalous subgraphs usually have large $\mathcal{X}^2(\widehat{S})$ values. Therefore, only the top-p abnormal subgraphs, identified based on their deviation from Benford's law, are selected as candidates for further consideration. This approach efficiently reduces computational overhead for subgraphs that conform to Benford's law. Additionally, the processes of k-ego net construction, peeling, and computing $\mathcal{X}^2(\widehat{S})$ are independent for different nodes, allowing for parallelization across multiple processors, making it highly efficient for large-scale financial networks.

Subsequently, the subgraph encoder, as formulated in Equation 2, is utilized to encode the graph structure of each subgraph $G[\widehat{S}]$ in $\mathcal{G}[\widehat{S}]$ into the vector space. Then the subgraphs $\mathcal{G}[\widehat{S}]$ whose embeddings are close to the encoded vectors of the training anomalous subgraphs $\mathcal{G}[S_{a_t}]$ are identified as coarse abnormal prototypes $\mathcal{G}[S_P]$. The details of the subgraph encoder and its optimization are illustrated below.

The subgraph encoder. To encode the hidden features in the *graph structure* of the subgraphs, we employ graph neural networks to model both the graph connectivity and the transaction frequency in the subgraphs simultaneously in an inductive learning way. Specifically, in each layer $l > 0$, the hidden feature of the node s is updated by the weighted features from its neighbors as follows:

$$f^{(l)}(s) = \sigma\left(\theta_1^{(l)} \cdot f^{(l-1)}(s) + \theta_2^{(l)} \cdot \sum_{j \in \mathcal{N}(s)} r_{j,s} \cdot f^{(l-1)}(j)\right), \tag{2}$$

where $r_{j,s}$ denotes the transaction frequency between nodes j and s (i.e., the number of transactions between j and s), and $\mathcal{N}(s)$ represents the neighbor set of the node s which reflects the graph connectivity. The parameters $\theta_1^{(l)}$ and $\theta_2^{(l)}$ are learnable weights in the neural networks.

Our goal is to align the embeddings of subgraphs with similar graph structures and financial distributions closely, while distancing the embeddings of subgraphs with differing structures and financial distributions. For each anomalous subgraph $G[S^i_{a_t}]$ in the training set of anomalous subgraphs $\mathcal{G}[S_{a_t}]$, we form positive subgraph pairs U. This is done by sampling two nested subgraphs $G[S^a] \subset G[S^b]$ from $G[S^i_{a_t}]$, ensuring that $e(G[S^a])_i \leq e(G[S^b])_i$ for each dimension i. The reason is that if $G[S^a]$ is a subgraph of $G[S^b]$, the embedding $e(G[S^a])_i$ must lie in the "lower-left" of the embedding $e(G[S^b])_i$ for each dimension i according to [15]. Conversely, negative subgraph pairs Z are constructed from two distinct anomalous subgraphs $G[S^j_{a_t}]$ and $G[S^k_{a_t}]$ such that $G[S^a] \nsubseteq G[S^b]$, $G[S^a] \subseteq G[S^j_{a_t}]$, and $G[S^b] \subseteq G[S^k_{a_t}]$, with both $G[S^j_{a_t}]$ and $G[S^k_{a_t}]$ belonging to $\mathcal{G}[S_{a_t}]$.

Contrasting with existing approaches such as those in [15, 28] that focus on only subgraph structures, our encoder uniquely incorporates the *financial distribution* aspect for modeling financial subgraphs. We utilize $D(G[S^a], G[S^b])$ to capture both the distance between the encoded vectors and the KL-divergence of financial distributions $w(G[S])$ between subgraph pairs as:

$$\begin{aligned} D(G[S^a], G[S^b]) = &|| \max\left\{0, e(G[S^a]) - e(G[S^b])\right\} ||_2^2 \\ &+ \text{ KL } \left(w(G[S^a]), w(G[S^b])\right) , \end{aligned} \tag{3}$$

where $|| \max\{\cdot\} ||_2^2$ measures the structural closeness between two subgraphs $G[S^a]$ and $G[S^b]$. And $e(G[S^a]) = \sum_{i \in G[S^a]} f^{(l)}(i)$ denotes the encoded vector of the subgraph $G[S^a]$ based on the hidden features of its nodes, where $e(G[S^a])_i \leq e(G[S^b])_i$ for each dimension i, if $G[S^a]$ is a subgraph of $G[S^b]$. Moreover, KL $(\cdot)$ represents the KL-divergence of financial distributions between two subgraphs $G[S^a]$ and $G[S^b]$. Subgraphs with similar financial distributions lead to lower KL scores.

Optimization of the subgraph encoder. The loss function is optimized by minimizing the distances between positive subgraph pairs and maximizing the distances between negative subgraph pairs as:

$$\begin{aligned} \mathcal{L} = &\sum_{G[S^a], G[S^b] \in U} D(G[S^a], G[S^b]) + \\ &\sum_{G[S^a], G[S^b] \in Z} \max\left\{0, \lambda - D(G[S^a], G[S^b])\right\} , \end{aligned} \tag{4}$$

where λ is the margin distance, and U and Z denote the sets of positive and negative subgraph pairs, respectively.

4.3 Anomalous Subgraph Refinement

State. The state at the i-th step includes $G[S_{P_i}]$ and its boundary $B_{S_{P_i}}$, with $G[S_{P_0}]$ representing the coarse abnormal prototypes from the prototype discovery module. The boundary $B_{S_{P_i}}$ consists of nodes directly connected to $G[S_{P_i}]$,

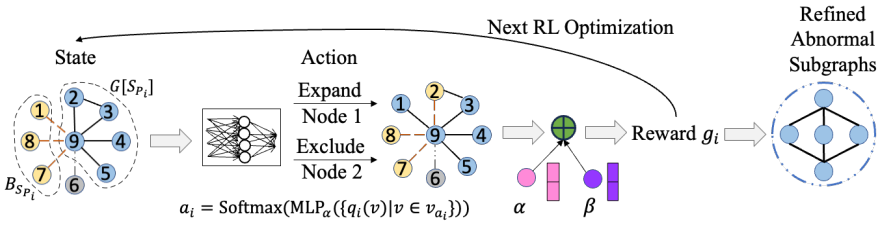

Fig. 4. The illustration of the anomalous subgraph refinement, where $G[S_{P_i}]$ denotes the prototype obtained by coarse prototype discovery in Sec. 4.2, $B_{S_{P_i}}$ denotes the boundary of the subgraph $G[S_{P_i}]$, and a_i is a function for deciding the action.

selected based on their aggregate transaction frequencies with nodes in $G[S_{P_i}]$. Specifically, we select the nodes that have the highest cumulative transaction frequency sum to nodes within $G[S_{P_i}]$, capped at m nodes. Formally, the boundary nodes are defined as:

$$B_{S_{P_i}} = \underset{I \subseteq V \setminus G[S_{P_i}]: |I| \leq m}{\arg\max} \sum_{s \in I} \sum_{c \in G[S_{P_i}]} r_{s,c} \ , \tag{5}$$

where $r_{s,c}$ denotes the transaction frequency between node s and node c, and the condition $|I| \leq m$ ensures that the number of nodes in the boundary does not exceed m.

To facilitate the actions that include or exclude nodes, we define the node representation of node v at the i+1-th step as follows:

$$q_{i+1}(v) = \text{concat}(f_\beta(v)_i, \mathbb{1}_{v \in G[S_{P_{i+1}}]}) \ , \tag{6}$$

where $f_\beta(v)_i$ denotes the node representation of v at the i-th step by the subgraph encoder in Equation 2, β denotes the trainable parameters. And $\mathbb{1}_{v \in G[S_{P_{i+1}}]}$ is the indicator function returning 1 if the condition satisfies, otherwise 0. Moreover, $G[S_{P_{i+1}}]$ denotes the subgraph $G[S_P]$ at the i+1-th step.

Action. The action space for the expansion action is the boundary nodes, while the action space for the exclusion action is the nodes in the current subgraphs. We propose to choose the boundary nodes as the ones with the most frequent transactions connecting with the current subgraphs. Specifically, in Figure 4, nodes 1, 7, and 8 have the top-3 transaction frequencies compared with node 6, so nodes 1, 7, and 8 are selected as the boundary $B_{S_{P_i}}$. At the i-th step, we take a node in $G[S_{P_i}]$ to exclude and a node in $B_{S_{P_i}}$ to expand, then we obtain $G[S_{P_{i+1}}]$. A virtual node is added to represent the stop action for both exclusion and expansion.

We apply a Multilayer Perceptron (MLP) to extract the hidden features behind the nodes in the action spaces, then map them into the probabilities of choosing specific nodes by softmax function for exclusion or expansion action.

For both exclusion and expansion actions, we check if these actions will lead to higher $\psi(S_{P_{i+1}})$ and $\mathcal{X}^2(S_{P_{i+1}})$ values, where $\psi(S_{P_{i+1}})$ is the average $\mathcal{X}^2$-statistic

of the subgraph $G[S_P]$ at the $i+1$-th step. If the conditions are satisfied, then the action will be conducted. Formally, the action is defined as:

$$\begin{aligned} Q_\alpha(v_{x_i}) = a_i = &\text{Softmax}(\text{MLP}_\alpha(\{q_i(v)|v \in v_{x_i}\})) \ , \\ &\text{s.t. } \psi(S_{P_{i+1}}) > \psi(S_{P_i}) \cap \\ &\mathcal{X}^2(S_{P_{i+1}}) > \mathcal{X}^2(S_{P_i}) \ , \end{aligned} \tag{7}$$

where v_{x_i} denotes the action space at the i-th step, which includes the boundary $B_{S_{P_i}}$ for expansion and the current subgraph $G[S_{P_i}]$ for exclusion, and $q_i(v)$ denotes the node representation of node v at the i-th step. The α denotes the trainable parameter in the MLP. Moreover, for exclusion action, we only exclude a node if removing it will not result in a disconnected subgraph.

Reward. In our RL framework, the objective is to refine abnormal subgraphs by maximizing the rewards yielded by the actions. The reward is quantified based on the abnormal degree of subgraphs following specific actions. We define the abnormal degree as:

$$d_a(S_{P_i}) = \frac{\psi(S_{P_i})}{\rho} \ , \tag{8}$$

where $\psi(S_{P_i})$ represents the average $\mathcal{X}^2$ per node of the subgraph $G[S_{P_i}]$, and $\rho = \frac{|E|}{|S|}$ is the density of the subgraph $G[S_{P_i}]$. According to prior research [3], an abnormal subgraph is indicated by a significantly higher $\psi(S_{P_i})$ compared to its density ρ. Therefore, the reward at each step is defined as the increase in the abnormal degree $d_a(S_{P_i})$ resulting from the chosen action. This approach encourages the model to steer the subgraph refinement towards conditions where $\psi(S_{P_i}) \gg \rho$, aligning with the criteria for abnormality.

Optimization. We formulate the problem as a maximization task with the aim of maximizing the rewards obtained through optimal actions, given by:

$$g_i = d_a(S_{P_{i+1}}) - d_a(S_{P_i}) \ , \tag{9}$$

where $d_a(S_{P_{i+1}})$ and $d_a(S_{P_i})$ represent the abnormal degrees of the subgraph $G[S_P]$ at the i+1-th and i-th steps, respectively.

Theorem 2. *The overall time complexity of the RADIO model is dominated by* $\mathcal{O}(deg_{\max}^k \cdot |V|)$*, where* $deg_{\max}$ *denotes the maximum degree of nodes, and* k *is the constant from* k*-ego net.*

5 Experiments

5.1 Experimental Setup

Datasets We evaluate all methods on four real financial datasets as in Table 1.

• The PlusTokenPonzi dataset [4] is a real Ethereum blockchain transaction dataset that involves money laundering activities from EthereumHeist [27]. It includes detailed information such as transaction timestamps and amounts, service provider address labels, hierarchical levels of laundering addresses, etc. This is the first publicly available dataset with ground truth data on money laundering.

• The ETH datasets, shared by Google BigQuery[5], contain Ethereum blockchain token transactions among addresses, including transaction amounts. These datasets are also used in AntiBenford [3].

Table 1. Statistics of experimented datasets.

Datasets	# Nodes	# Edges	# Transactions
PlusTokenPonzi	38,324	58,731	64,858
ETH-Jan-2018	1,761,571	2,749,707	4,279,799
ETH-Jan-2019	2,199,347	3,331,594	6,128,061
Blur	175,071	1,103,791	3,539,773

• The Blur dataset is a transaction dataset from the NFT marketplace [32], which is compiled by Etherscan API [6] from Oct. 19, 2022 to Apr. 1, 2023. They contain NFT transactions among addresses.

Preprocessing Consistent with AntiBenford [3], transactions valued at less than 1 unit in ETH datasets are excluded during preprocessing. Multiple transactions between two nodes are represented as a single edge, with transaction frequency and the financial distribution (probabilities of transaction amounts starting with digit o). Since ETH and Blur datasets lack inherent anomaly labels, we randomly pick 60 anomalies identified by the SOTA [3] as the training set as in [28]. Since the PlusTokenPonzi dataset already contains anomaly labels, we randomly select 20%, 10%, and 70% of the ground truth data as the training set, validation set, and testing set, respectively.

Competitors We compare our proposed RADIO with twelve methods.

Non-learning-based anomaly detection methods: The SOTA method **AntiBenford** [3], **FlowScope** [12] and **Holoscope** [13].

Learning-based anomaly detection methods: **CLARE** [28], **BigClam** [29], **CPM** [21], **AS-GAE** [31], **GCAD** [33] and **SIGNET** [14].

Densest subgraph discovery methods: **Density-Friendly** [4], **Core-Approx** [18] and **KS-Approx** [10].

Hyperparameter Settings We conduct hyperparameter learning using grid search. We set the margin $\lambda = 0.4$ as [28], and tune the maximum size m of

[4]https://github.com/lindan113/EthereumHeist?tab=readme-ov-file

[5]https://www.kaggle.com/bigquery/ethereum-blockchain

[6]https://etherscan.io/

nodes in the boundary in {100, 150, 200, 250}, the size of the top-p candidates in {10, 50, 100, 200}, the depth l of the graph neural networks in {2, 3, 4, 5, 6}, and the layer of the k-ego net in {1, 3, 5, 7}.

Performance Metrics We evaluate performance by standard metrics as [3]: $\mathcal{X}^2(S)$, the density ρ, and $\psi(S)$. The $\mathcal{X}^2(S)$ evaluates the deviation from Benford's law, while $\psi(S)=\frac{\mathcal{X}^2(S)}{|S|}$ calculates the average deviation, allowing fair comparisons across subgraphs of varying sizes. Since a subgraph is considered abnormal if $\psi(S) \gg \rho$ [3], we use the abnormal degree $d_a(S) = \frac{\psi(S)}{\rho}$ as a metric.

Since the PlusTokenPonzi dataset includes ground truth data, we evaluate the similarity between detected anomalies and the ground truth using the ONMI (Overlapping Normalized Mutual Information) metric as in [28, 20], which is an overlapping version of the NMI score.

Table 2. Effectiveness on PlusTokenPonzi. For each method, we report average results over five runs. Note that the best method should extract subgraphs with higher abnormal degree $d_a(S)$ and relatively higher density ρ.

top-a	Metrics	Density-Friendly	KS-Approx	Core-Approx	CPM	BigClam	CLARE	AS-GAE	GCAD	SIGNET	Holoscope	FlowScope	AntiBenford	RADIO
5	$\mathcal{X}^2(S)$	5513.34	1396.12	1113.94	1706.51	1077.43	1853.39	562.52	2707.42	1523.07	988.29	1888.61	4342.65	**7458.96**
	$\psi(S)$	226.83	12.52	30.31	10.74	14.97	13.03	16.83	12.92	13.28	12.26	13.16	23.83	**942.02**
	ρ	**289.94**	15.19	23.18	29.87	16.74	27.60	25.90	24.00	28.99	32.14	12.27	18.89	67.36
	$d_a(S)$	0.78	0.82	1.31	0.36	0.89	0.47	1.20	0.54	0.46	0.38	1.07	1.26	**13.98**
	ONMI	0.30	0.31	0.49	0.34	0.51	0.39	0.55	0.49	0.31	0.22	0.45	0.44	**0.81**
10	$\mathcal{X}^2(S)$	3605.81	2288.54	975.37	1430.38	1129.09	1259.05	344.58	1789.41	1227.62	236.12	1887.88	3357.24	**6967.22**
	$\psi(S)$	174.18	7.33	22.69	21.85	11.21	10.04	11.99	11.30	12.66	12.15	12.01	14.82	**648.83**
	ρ	**195.14**	26.21	17.07	21.02	12.33	22.41	11.49	20.91	25.26	27.87	10.38	16.53	36.99
	$d_a(S)$	0.89	0.28	1.33	1.04	0.91	0.45	1.27	0.54	0.50	0.44	1.16	0.90	**17.54**
	ONMI	0.29	0.21	0.43	0.30	0.42	0.31	0.49	0.38	0.25	0.10	0.44	0.38	**0.78**
15	$\mathcal{X}^2(S)$	2202.56	1501.55	864.74	950.58	598.79	963.15	234.53	1516.76	1187.95	124.61	736.18	2980.54	**6437.85**
	$\psi(S)$	115.31	3.55	21.06	17.43	10.40	8.01	9.95	9.68	10.42	9.46	8.48	17.06	**510.31**
	ρ	**129.05**	4.84	14.63	19.00	10.56	17.21	8.84	20.10	24.28	17.70	15.35	19.02	24.49
	$d_a(S)$	0.89	0.73	1.44	0.92	0.98	0.47	0.86	0.48	0.43	0.53	0.55	0.90	**20.84**
	ONMI	0.22	0.21	0.39	0.29	0.40	0.26	0.44	0.32	0.21	0.00	0.38	0.30	**0.67**
20	$\mathcal{X}^2(S)$	1760.02	21.77	296.01	494.36	510.56	438.70	159.05	1227.78	935.97	103.65	746.88	1973.69	**6123.21**
	$\psi(S)$	64.48	1.53	17.96	7.86	8.87	6.83	6.91	4.24	8.04	7.23	6.31	4.42	**326.56**
	ρ	**54.91**	2.02	14.49	17.22	10.47	13.33	7.61	14.23	17.19	16.85	8.77	4.93	16.55
	$d_a(S)$	1.17	0.76	1.24	0.46	0.85	0.51	0.87	0.30	0.47	0.43	0.72	0.90	**19.73**
	ONMI	0.11	0.21	0.32	0.22	0.32	0.21	0.32	0.18	0.17	0.00	0.33	0.23	**0.50**

5.2 Effectiveness Evaluation

We evaluate the effectiveness of all methods in Tables 2, 3, 4, and 5, ranking subgraphs by $\psi(S)$. Ranking by $d_a(S)$ would place subgraphs with very low density ρ at the top (since $d_a(S) = \frac{\psi(S)}{\rho}$), but these subgraphs are not dense and do not meet the definition of anomalous subgraphs. We observe:

(1) RADIO beats other methods on the PlusTokenPonzi dataset when compared to the ground truth, which achieves the highest ONMI scores. This demonstrates its superior accuracy in anomaly detection.

(2) RADIO consistently outperforms competitors in $\psi(S)$ values and in most cases in $d_a(S)$ values. The exception is CLARE on the ETH-JAN-2018 dataset in the top 5, where it gives a higher $d_a(S)$ but with a density ρ below 1, indicating the subgraph is not dense.

Table 3. Effectiveness on ETH-Jan-2018.

top-a	Metrics	Density-Friendly	KS-Approx	Core-Approx	CPM	BigClam	CLARE	AS-GAE	GCAD	SIGNET	Holoscope	FlowScope	AntiBenford	RADIO
5	$\mathcal{X}^2(S)$	1342.96	1226.12	2400.03	120.91	54.78	57.425	335.70	540.83	963.15	236.88	4836.59	**52669.68**	34627.48
	$\psi(S)$	431.47	0.41	0.08	24.30	3.66	1.132	4.44	7.81	6.12	25.93	112.56	15.94	**7479.48**
	ρ	**6456.58**	1.72	2.86	77.88	1.56	0.201	36.70	19.54	9.41	19.96	386.69	6.24	1828.24
	$d_a(S)$	0.07	0.24	0.03	0.31	2.35	**5.63**	0.12	0.40	0.65	1.30	0.29	2.55	4.09
10	$\mathcal{X}^2(S)$	803.13	666.10	1564.63	82.57	62.33	35.74	198.40	320.93	556.81	630.67	3215.98	**26678.33**	19206.94
	$\psi(S)$	226.37	0.21	0.05	15.68	2.58	0.61	2.97	4.86	3.50	15.96	60.29	11.34	**3779.10**
	ρ	**3479.54**	1.01	1.60	44.57	1.27	0.31	19.96	15.33	8.46	11.42	316.52	19.89	1019.64
	$d_a(S)$	0.07	0.21	0.03	0.35	2.03	1.96	0.15	0.32	0.41	1.40	0.19	0.57	**3.71**
15	$\mathcal{X}^2(S)$	616.43	467.19	1082.84	59.74	92.55	26.36	173.14	229.02	387.46	468.69	2686.79	**18017.14**	13027.78
	$\psi(S)$	152.94	0.14	0.03	11.52	1.99	0.20	2.23	3.61	2.49	12.56	43.69	9.33	**2530.46**
	ρ	**2339.56**	0.71	1.13	33.42	1.46	0.22	21.68	12.71	6.89	20.97	317.52	15.15	759.22
	$d_a(S)$	0.07	0.20	0.03	0.34	1.36	0.93	0.10	0.28	0.36	0.60	0.14	0.62	**3.33**
20	$\mathcal{X}^2(S)$	474.34	353.95	825.36	47.48	88.19	25.48	138.36	177.69	295.54	369.87	2491.58	**13528.65**	10563.19
	$\psi(S)$	115.68	0.11	0.03	9.23	1.89	0.40	1.75	2.84	1.92	9.82	37.06	8.04	**1903.35**
	ρ	**1775.76**	0.54	0.87	28.13	1.51	0.21	17.23	10.23	5.49	18.23	322.03	11.67	570.67
	$d_a(S)$	0.07	0.20	0.03	0.33	1.25	1.94	0.10	0.28	0.35	0.54	0.12	0.69	**3.34**

Table 4. Effectiveness on ETH-Jan-2019 dataset.

top-a	Metrics	Density-Friendly	KS-Approx	Core-Approx	CPM	BigClam	CLARE	AS-GAE	GCAD	SIGNET	Holoscope	FlowScope	AntiBenford	RADIO
5	$\mathcal{X}^2(S)$	1889.95	149.38	20.17	3746.68	1011.23	3879.66	7390.42	718.43	1269.55	1921.88	10987.22	11368.72	**31282.82**
	$\psi(S)$	695.16	8.52	2.25	573.68	5.12	50.50	53.84	6.80	10.42	20.63	290.33	84.93	**3641.20**
	ρ	1665.80	33.69	1.33	**3728.06**	12.98	59.91	84.38	8.52	13.51	18.01	345.36	18.93	341.13
	$d_a(S)$	0.42	0.25	1.69	0.15	0.39	0.84	0.64	0.80	0.77	1.15	0.84	4.49	**10.66**
10	$\mathcal{X}^2(S)$	1511.78	2301.39	45.96	2147.24	1599.52	3574.93	4215.11	449.49	808.07	10155.63	6155.96	6000.45	**24983.13**
	$\psi(S)$	473.36	5.81	1.74	307.93	3.87	36.72	32.95	4.71	7.28	16.99	154.12	44.22	**2482.06**
	ρ	987.54	28.86	1.20	**1988.23**	7.01	50.24	56.75	6.86	20.66	13.20	173.34	11.83	236.42
	$d_a(S)$	0.48	0.20	1.45	0.15	0.55	0.73	0.58	0.69	0.35	1.29	0.89	3.74	**10.49**
15	$\mathcal{X}^2(S)$	1147.46	5669.96	82.00	1464.12	2396.14	3320.04	2812.28	347.39	601.81	966.53	4375.22	7353.90	**21989.41**
	$\psi(S)$	365.65	4.08	1.38	211.38	2.69	30.65	22.08	3.55	5.70	15.19	107.39	30.21	**1799.47**
	ρ	713.58	21.66	1.42	**1335.52**	5.13	43.71	37.95	7.93	17.05	9.27	177.98	111.32	173.73
	$d_a(S)$	0.51	0.19	0.97	0.16	0.52	0.70	0.58	0.45	0.33	1.64	0.60	0.27	**10.35**
20	$\mathcal{X}^2(S)$	1040.15	114.99	77.26	1121.52	1794.22	2929.98	2109.21	278.52	475.83	852.55	3699.97	8602.36	**19340.37**
	$\psi(S)$	298.89	3.83	1.32	162.07	2.19	25.67	16.56	2.85	4.64	12.63	90.89	22.90	**1399.17**
	ρ	577.53	20.31	1.39	**1009.12**	4.93	40.15	28.46	7.02	19.54	7.11	149.55	84.42	138.11
	$d_a(S)$	0.52	0.19	0.95	0.16	0.44	0.64	0.58	0.41	0.24	1.78	0.61	0.27	**10.12**

(3) Although methods like Density-Friendly and CPM give higher densities ρ, their $d_a(S)$ values are below 1, indicating the subgraphs are not abnormal according to [3]. RADIO produces denser subgraphs with higher $d_a(S)$.

Table 5. Effectiveness on Blur dataset.

top-a	Metrics	Density-Friendly	KS-Approx	Core-Approx	CPM	BigClam	CLARE	AS-GAE	GCAD	SIGNET	Holoscope	FlowScope	AntiBenford	RADIO
5	$\mathcal{X}^2(S)$	12967.19	3666.68	642.53	272.12	3594.68	4085.12	441.59	161.39	97.43	507.94	151.74	640.74	**16731.76**
	$\psi(S)$	632.83	6.46	0.90	0.82	1.42	25.55	0.58	1.15	0.98	1.31	0.70	2.71	**1208.83**
	ρ	**338.93**	8.25	0.91	0.77	0.94	14.79	1.44	1.38	1.57	1.19	0.69	1.17	190.05
	$d_a(S)$	1.87	0.78	0.98	1.06	1.52	1.73	0.40	0.83	0.62	1.10	1.01	2.31	**6.36**
10	$\mathcal{X}^2(S)$	6961.97	5844.11	487.37	213.19	1886.41	2459.32	321.94	146.85	70.80	173.57	109.85	343.40	**21492.51**
	$\psi(S)$	390.31	4.82	0.53	0.71	1.11	16.27	0.33	0.82	0.53	0.81	0.65	1.94	**717.78**
	ρ	**198.61**	7.44	0.59	0.69	0.73	9.02	1.39	1.69	1.45	1.39	0.50	0.96	130.63
	$d_a(S)$	1.97	0.65	0.90	1.02	1.52	1.80	0.24	0.48	0.37	0.58	1.30	2.02	**5.49**
15	$\mathcal{X}^2(S)$	5696.43	7033.36	449.58	180.47	1495.84	1786.01	296.21	186.45	72.18	108.06	105.75	259.30	**19166.75**
	$\psi(S)$	280.53	3.66	0.82	0.47	0.99	12.20	0.30	0.62	0.52	0.55	0.36	1.59	**539.14**
	ρ	**163.66**	6.18	0.78	0.45	0.63	6.81	1.31	1.38	1.14	1.08	0.87	0.85	115.50
	$d_a(S)$	1.71	0.59	1.05	1.05	1.57	1.79	0.23	0.45	0.46	0.51	0.41	1.86	**4.67**
20	$\mathcal{X}^2(S)$	4509.07	7158.29	734.53	162.71	1140.31	1373.43	214.83	144.91	54.54	89.99	65.39	223.07	**15332.66**
	$\psi(S)$	217.20	2.93	0.83	0.37	0.86	9.70	0.22	0.72	0.36	0.53	0.39	1.39	**424.87**
	ρ	**136.43**	5.48	1.22	0.66	0.63	5.34	1.72	1.67	1.26	1.02	0.52	0.80	94.41
	$d_a(S)$	1.59	0.53	0.68	0.56	1.36	1.82	0.13	0.43	0.28	0.52	0.76	1.74	**4.50**

(4) Since AntiBenford obtains one subgraph in the top 5 with extremely large $\mathcal{X}^2(S)$ on ETH-JAN-2018, i.e., 2.59e5, the average values of $\mathcal{X}^2(S)$ in all top-a cases are significantly larger than other methods. The reason for this large $\mathcal{X}^2(S)$ is that the size of nodes in this subgraph is very large, i.e., 7245. It results in a low $\psi(S)$, i.e., 35.75, which means that average anomaly per node is low.

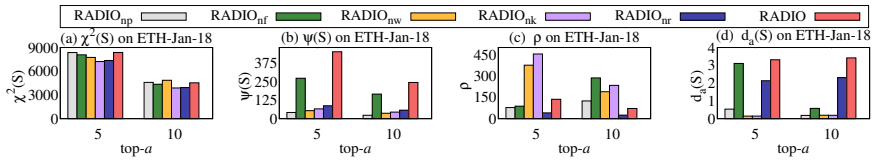

Fig. 5. The ablation study w.r.t. four evaluation metrics.

5.3 Ablation Study

We conduct an ablation study in Figure 5, omitting the PlusTokenPonzi, ETH-Jan-19, Blur datasets and results of top-15 and 20 due to similar behaviors. RADIO$_{\mathbf{nr}}$ ignores anomalous subgraph refinement (Section 4.3). RADIO$_{\mathbf{nw}}$ ignores weights, i.e., transaction frequency, for the subgraph encoder (Section 4.2). RADIO$_{\mathbf{nk}}$ removes the KL-divergence of financial distributions between pairs (Section 4.2). RADIO$_{\mathbf{np}}$ omits the peeling process (Section 4.2). RADIO$_{\mathbf{nf}}$ randomly samples connected nodes as the boundary nodes (Section 4.3). We observe:

(1) RADIO beats RADIO$_{\mathbf{nr}}$ on ETH-Jan-18, showing the importance of anomalous subgraph refinement for enhancing prototypes toward the abnormal direction.

(2) Although RADIO$_{\mathbf{nw}}$ achieves higher density ρ, it results in a very low abnormal degree $d_a(S)$, indicating the dense subgraph is not abnormal. This confirms the importance of using transaction frequency in the subgraph encoder.

(3) Although RADIO$_{\mathbf{nk}}$ gets higher ρ, it returns subgraphs with very low $d_a(S)$. It highlights the importance of using KL-divergence between subgraph pairs in learning transaction similarity.

(4) RADIO significantly outperforms RADIO$_{\mathbf{np}}$. This highlights the importance of fast densest subgraph discovery by peeling.

(5) RADIO outperforms RADIO$_{\mathbf{nf}}$. Although RADIO$_{\mathbf{nf}}$ has higher density ρ, their low $d_a(S)$ indicates the subgraphs are normal. It confirms the importance of selecting nodes with the most frequent transactions as boundaries.

5.4 Efficiency Evaluation

We use Intel Xeon Platinum 8370C processor 32-core 2.8GHz CPU with NVIDIA GeForce RTX 4090 24G GPU for evaluation. Figure 6 (a) shows the average detection time for discovering 40 abnormal subgraphs and Figure 6 (b) shows the average training time. The PlusTokenPonzi dataset is omitted due to a similar trend. CPM and BigClam run faster in the detection phase because they do not involve financial distribution computation. Although RADIO is slower than them, it discovers more abnormal subgraphs. Moreover, the training time of our proposed RADIO model is relatively shorter compared to most methods.

We evaluate the running time as the number of abnormal subgraphs varies from 50 to 1600 in Figure 7, omitting the PlusTokenPonzi and Blur datasets due to its similar trend to the ETH datasets. Density-Friendly and CPM run faster

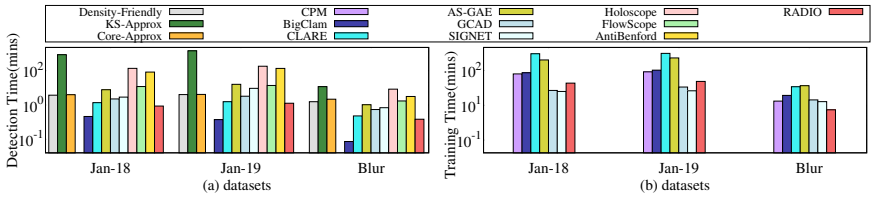

Fig. 6. (a) Detection time; (b) training time. Note that training times of non-learning-based methods are 0.

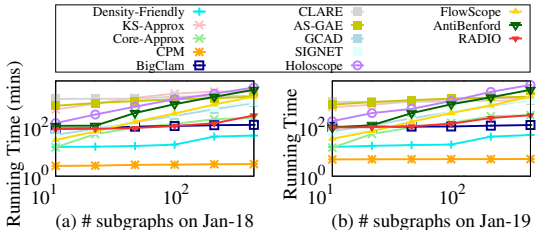

Fig. 7. Efficiency w.r.t. (a) # abnormal subgraphs on ETH-Jan-18, (b) ETH-Jan-19.

as they do not involve financial distribution computation. RADIO outperforms most competitors in speed as the size of abnormal subgraphs increases.

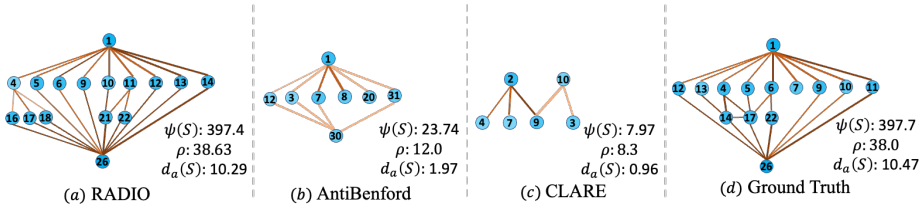

Fig. 8. Case Study on (a) RADIO; (b) AntiBenford; (c) CLARE, with the ground truth shown in (d). The edge color indicates transaction frequency.

5.5 Case Study

We analyze the interpretability of RADIO by showing the detected abnormal subgraphs on the PlusTokenPonzi dataset in Figure 8 (a). The smurf-like structure identified by RADIO is commonly associated with money laundering schemes [11, 23]. Its overlapping ratio with the ground truth, shown in Figure 8 (d), is 61.9%. Additionally, the values of density ρ and abnormal degree $d_a(S)$ are very close to those of the ground truth. For comparison, the abnormal subgraphs detected by AntiBenford and CLARE are displayed in Figure 8 (b–c), with

overlapping ratios of only 20% and 22.2%, respectively. RADIO outperforms these methods by effectively capturing transaction distributions among nodes and refining candidates in the direction of the most abnormal patterns.

6 Conclusions

In this paper, we tackle the challenge of detecting anomalous subgraphs in financial networks. Firstly, coarse prototypes are detected by matching trained anomalies via an efficient pruning strategy. We then refine the subgraphs using a reinforcement learning-based approach, scoping the subgraph boundary based on financial frequencies. Our extensive evaluation shows that RADIO is more effective than state-of-the-art models. Furthermore, RADIO is efficient when applied to large networks with millions of nodes.

Acknowledgement

This work is supported in part by NSFC [62433016, 62302397, 62302421, 62102321], the fund of Laboratory for Advanced Computing and Intelligence Engineering (No. 2023-LYJJ-01-021), Fundamental Research Funds for the Central Universities, China under Grant No. D5000230191, Basic and Applied Basic Research Fund in Guangdong Province under Grant 2023A1515011280, Ant Group through CCF-Ant Research Fund, Shenzhen Research Institute of Big Data under grant SIF20240004, the Guangdong Provincial Key Laboratory of Big Data Computing, The Chinese University of Hong Kong, Shenzhen, and CCF-Zhipu Large Model Innovation Fund under Grant No. CCF-Zhipu202413.

References

1. Benford, F.: The law of anomalous numbers. Proceedings of the American philosophical society pp. 551–572 (1938)
2. Charikar, M.: Greedy approximation algorithms for finding dense components in a graph. In: APPROX. pp. 84–95. Springer (2000)
3. Chen, T., Tsourakakis, C.: Antibenford subgraphs: Unsupervised anomaly detection in financial networks. In: SIGKDD. pp. 2762–2770 (2022)
4. Danisch, M., Chan, T.H.H., Sozio, M.: Large scale density-friendly graph decomposition via convex programming. In: WWW. pp. 233–242 (2017)
5. Fang, Y., Yu, K., Cheng, R., Lakshmanan, L.V., Lin, X.: Efficient algorithms for densest subgraph discovery. PVLDB (2019)
6. Han, X., Cheng, R., Grubenmann, T., et al.: Leveraging contextual graphs for stochastic weight completion in sparse road networks. In: SIAM SDM (2022)
7. Han, X., Cheng, R., Ma, C., Grubenmann, T.: Deeptea: Effective and efficient online time-dependent trajectory outlier detection. VLDB **15**(7), 1493–1505 (2022)
8. Han, X., Grubenmann, T., Cheng, R., Wong, S.C., Li, X., Sun, W.: Traffic incident detection: A trajectory-based approach. In: ICDE. pp. 1866–1869. IEEE (2020)
9. Han, X., Grubenmann, T., Ma, C., et al.: Fdm: Effective and efficient incident detection on sparse trajectory data. Information Systems p. 102418 (2024)

10. Khuller, S., Saha, B.: On finding dense subgraphs. In: ICALP. pp. 597–608. Springer (2009)
11. Lee, M.C., Zhao, Y., Wang, A., Liang, P.J., Akoglu, L., Tseng, V.S., Faloutsos, C.: Autoaudit: Mining accounting and time-evolving graphs. In: Big Data (2020)
12. Li, X., Liu, S., Li, Z., Han, X., Shi, C., Hooi, B., Huang, H., Cheng, X.: Flowscope: Spotting money laundering based on graphs. In: AAAI. vol. 34 (2020)
13. Liu, S., Hooi, B., Faloutsos, C.: Holoscope: Topology-and-spike aware fraud detection. In: CIKM. pp. 1539–1548 (2017)
14. Liu, Y., Ding, K., Lu, Q., Li, F., Zhang, L.Y., Pan, S.: Towards self-interpretable graph-level anomaly detection. NeurIPS **36** (2024)
15. Lou, Z., You, J., et al.: Neural subgraph matching. arXiv preprint arXiv:2007.03092 (2020)
16. Ma, C., Cheng, R., Lakshmanan, L.V., Han, X.: Finding locally densest subgraphs: a convex programming approach. VLDB **15**(11), 2719–2732 (2022)
17. Ma, C., Fang, Y., Cheng, R., Lakshmanan, L.V., Han, X.: A convex-programming approach for efficient directed densest subgraph discovery. In: SIGMOD (2022)
18. Ma, C., Fang, Y., Cheng, R., Lakshmanan, L.V., et al.: Efficient algorithms for densest subgraph discovery on large directed graphs. In: SIGMOD (2020)
19. Ma, C., Fang, Y., Cheng, R., Lakshmanan, L.V., et al.: Accelerating directed densest subgraph queries with software and hardware approaches. VLDBJ **33**(1) (2024)
20. McDaid, A.F., Greene, D., Hurley, N.: Normalized mutual information to evaluate overlapping community finding algorithms. arXiv preprint arXiv:1110.2515 (2011)
21. Palla, G., Derényi, I., Farkas, I., Vicsek, T.: Uncovering the overlapping community structure of complex networks in nature and society. nature **435**(7043) (2005)
22. Prakash, B.A., Sridharan, A., et al.: Eigenspokes: Surprising patterns and scalable community chipping in large graphs. In: PAKDD. pp. 435–448 (2010)
23. Starnini, M., Tsourakakis, et al.: Smurf-based anti-money laundering in time-evolving transaction networks. In: ECML PKDD. pp. 171–186. Springer (2021)
24. Sun, F.Y., Qu, M., Hoffmann, J., Huang, C.W., et al.: vgraph: A generative model for joint community detection and node representation learning. NeurIPS (2019)
25. Wang, Y., Liu, X., Shen, Y., Song, X., Wang, T., Shang, X., Peng, J.: Collaborative deep learning improves disease-related circrna prediction based on multi-source functional information. Briefings in bioinformatics **24**(2), bbad069 (2023)
26. Wang, Y., Shen, W., Shen, Y., Feng, S., Wang, T., et al.: Integrative graph-based framework for predicting circrna drug resistance using disease contextualization and deep learning. IEEE Journal of Biomedical and Health Informatics (2024)
27. Wu, J., Lin, D., Fu, Q., et al.: Toward understanding asset flows in crypto money laundering through the lenses of ethereum heists. TIFS **19** (2024)
28. Wu, X., Xiong, Y., Zhang, Y., Jiao, Y., Shan, C., Sun, Y., Zhu, Y., Yu, P.S.: Clare: A semi-supervised community detection algorithm. In: SIGKDD (2022)
29. Yang, J., Leskovec, J.: Overlapping community detection at scale: a nonnegative matrix factorization approach. In: WSDM. pp. 587–596 (2013)
30. Zhang, Y., Xiong, Y., Ye, Y., et al.: Seal: Learning heuristics for community detection with generative adversarial networks. In: SIGKDD. pp. 1103–1113 (2020)
31. Zhang, Z., Zhao, L.: Unsupervised deep subgraph anomaly detection. In: 2022 IEEE International Conference on Data Mining (ICDM). pp. 753–762 (2022)
32. Zhou, C., Chen, H., Wu, H., Zhang, J., Cai, W.: Artemis: Detecting airdrop hunters in nft markets with a graph learning system. In: WWW. pp. 1824–1834 (2024)
33. Zhuang, Z., Ting, K.M., Pang, G., Song, S.: Subgraph centralization: A necessary step for graph anomaly detection. In: SIAM SDM. pp. 703–711. SIAM (2023)